

Chapter 2

Liquefaction

Contents

2.1	Introduction	7
2.2	Observations in the Near Field	9
2.3	Laboratory Studies	11
2.3.1	Cyclic Loading Experiments	14
2.3.2	Dissipated Energy for Liquefaction by Undrained Consolidation	15
2.4	Liquefaction Beyond the Near Field	15
2.4.1	Seismic Energy Density as a Metric for Liquefaction Distribution	16
2.4.2	Mechanism for Liquefaction Beyond the Near Field	18
2.5	Experiment at Wildlife Reserve, California	19
2.6	Dependence of Liquefaction on Seismic Frequency	24
2.6.1	Field Observation from Taiwan	24
2.6.2	Laboratory Studies	27
2.6.3	Numerical Models	28
2.7	Concluding Remarks	29
	References	29

2.1 Introduction

In 373/2 BC Helice, a coastal town in ancient Greece, disappeared entirely under the sea after being leveled by a great earthquake. In 1861, the same place was hit by another earthquake, though to a lesser degree. Schmidt (1875) studied the affected area and showed extensive lateral spreading and subsidence of land along the coast (Fig. 2.1). Similar phenomena were documented along the coast near Anchorage, Seward and Valdez following the 1964 M9.2 Alaska earthquake (see Sect. 2.2), where the slumping of land was shown to be caused by the liquefaction of soft clays and sands underneath a gentle slope (Seed, 1968).

Liquefaction is a process by which the rigidity of saturated sediments is reduced to zero and the sediments become fluid-like. It occurs mostly during earthquakes and is invariably associated with high pore-water pressure, as evidenced by the common

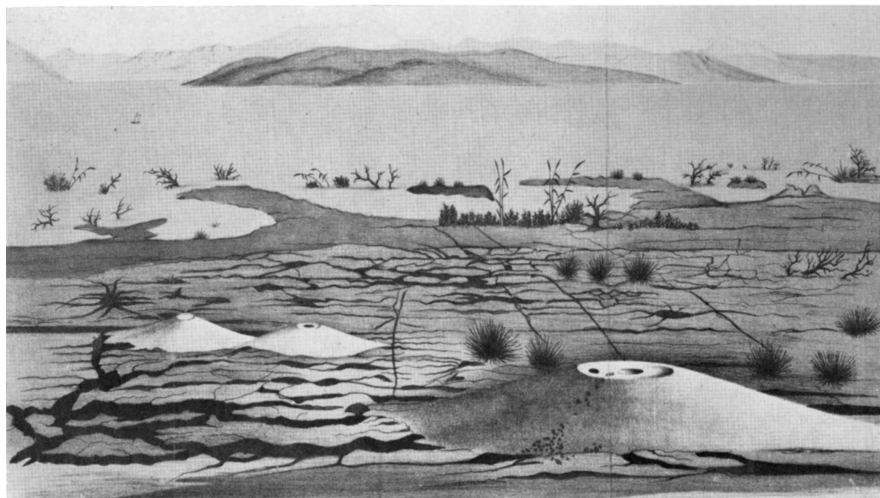


Fig. 2.1 Drawing shows the affected area of Helice after the earthquake of 1861. In the foreground, the remaining part of the land was broken into a collage of many irregular pieces separated by a patchwork of extensional fractures, covered sparingly by sand-craters. Off the coast in the Gulf of Corinth, tree tops marked part of the submerged strip of coastal plain. (From Marinatos, 1960)

occurrence of ejections of water and sediments to substantial height during liquefaction (Fig. 2.2). Eyewitnesses to the great 1964 Alaska earthquake at distances up to 400 km from the epicenter, for example, reported that eruptions of water and sediments reached heights up to 30 m (Waller, 1966).

In addition to being a significant hydrogeologic process in its own right, liquefaction has drawn much attention from engineers because it can create great damage to man-made structures. It causes ground to subside and to spread laterally, thus induces buildings to tilt, damages airport runways and earth embankments, and disrupts buried pipes and pile foundations. Since the 1960s, earthquake engineers have carried out a great amount of research to study liquefaction and to predict its occurrence. Their works are summarized in several special volumes (e.g., National Research Council, 1985; Pitilakis, 2007) and will not be repeated here. Only the results critical to the understanding of the interaction between earthquakes and water are summarized in Sect. 2.3.

The engineering approach to study liquefaction has been based on the principle of effective stress (Appendix D, Eq. D.1 and D.2), first proposed by Terzaghi (1925). Based on this concept, liquefaction is a consequence of pore-pressure increase when sediments consolidate in an ‘undrained’ condition during earthquakes (see Sect. 2.3). When pore pressure becomes so high that the effective stress is reduced to zero, sediments become fluid-like, i.e., liquefy. Recent investigation (Wang, 2007) shows, however, that ‘undrained’ consolidation of sediments may occur only in the near field of an earthquake; beyond the near field the seismic energy density may be too small to initiate consolidation, even in the most sensitive sediments (Sect. 2.4.1).



Fig. 2.2 Smear *left* on a building wall created by ejected sand during the 1999 M 7.5 Chi-Chi earthquake in Taiwan. Motorcycle at lower *left* shows scale (From Su et al., 2000)

A new mechanism may thus be required to explain the great number of liquefaction examples that have been documented beyond the near field (Fig. 2.6; Sect. 2.4.2).

In Sect. 2.5, we discuss the dependence of liquefaction on the frequency of the seismic waves. This issue is important but has been scarcely studied until recently. We emphasize that the results remain controversial and require more research in the future.

2.2 Observations in the Near Field

One of the best studied regions for liquefaction features is the New Madrid Seismic Zone in the central United States (Fig. 2.3), where widespread liquefaction was induced by nearby historic and prehistoric earthquakes. Liquefaction features, mapped over several thousand square kilometers (Obermeir, 1989), are present in various shapes, sizes, and ages. Many surficial vented deposits, or sand blows, are 1.0–1.5 m in thickness and 10–30 m in diameter and are still easy to identify on the ground surface and on aerial photographs and satellite images despite years of modification by active agricultural activities (Tuttle and Schweig, 1996). Sand dikes, which represent the conduits for escaping pore water and sediments from the liquefied layers below the sand blows, are also abundant. Most of these features are thought to have formed during the 1810–1811 M8 New Madrid earthquakes, even though many may be prehistoric in age (Tuttle and Schweig, 1996).

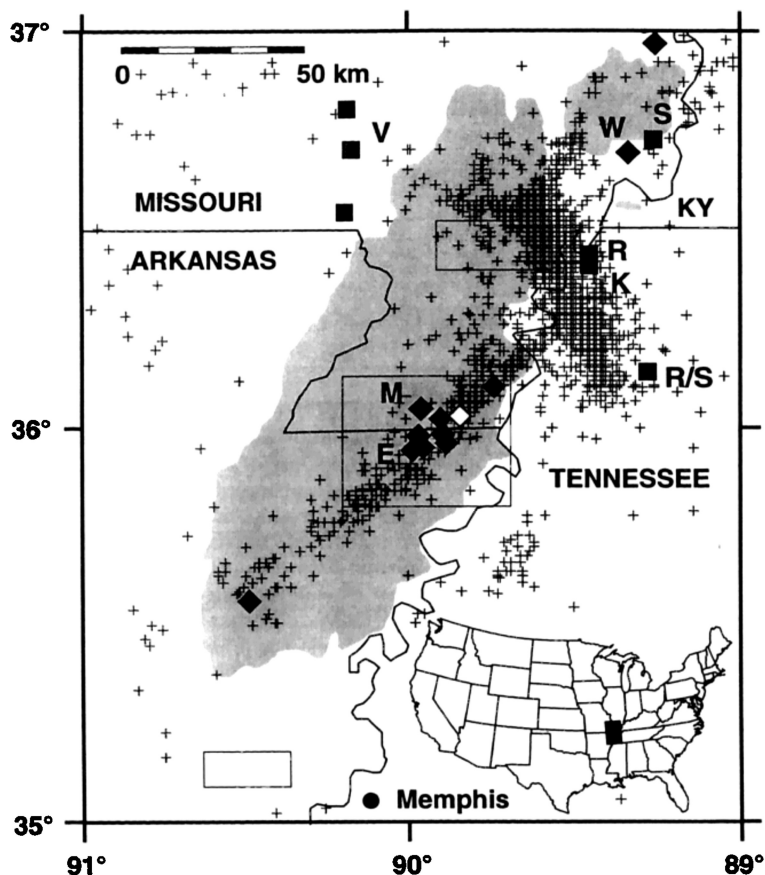


Fig. 2.3 Location map of showing the liquefaction sites within the New Madrid seismic zone. *Shaded area* represents the area where >1% of the ground surface is covered by sand-blow deposits (Obermeir, 1989). Seismicity (1974–1991), shown by *crosses*, defines the New Madrid Seismic Zone. *Symbols and letters* refer to sites of previous liquefaction and paleoliquefaction studies (From Tuttle and Schweig, 1996)

Two earthquake events are particularly important in bringing liquefaction phenomena and their devastating effects to the attention of engineers and seismologists. This awareness has in turn led to a great amount of research during the past 50 years in an effort to better understand liquefaction and to mitigate its damage.

The 1964 M9.2 Alaska earthquake occurred at a depth of approximately 30 km beneath Prince William Sound; the rupture extended laterally for 800 km parallel to the Aleutian trench and uplifted about 520,000 km² of the crust. Many landslides occurred; the most spectacular slide took place at the Turnagain Height area of Anchorage, caused by liquefaction of the underlying soft clay and sands. The slide extended ~2800 m laterally along a bluff and continued inland for an average distance of ~300 m, resulting in 130 acres of land sliding toward the ocean (Seed, 1968). Within the slide area the ground was broken into blocks that collapsed and tilted at all angles forming a chaotic collage of ridges and depressions.



Fig. 2.4 Tilted apartment buildings after the Niigata earthquake. Despite the extreme tilting, the buildings themselves suffered remarkably little structural damage (From the Earthquake Engineering Research Center Library, University of California at Berkeley)

In the depressed areas, the ground dropped an average of 12 m during the sliding. Houses in the area, some of which moved laterally as much as 150 or 180 m, were completely destroyed.

During the 1964 M7.5 Niigata Earthquake, Japan, dramatic damage was caused by liquefaction of the sand deposits in the low-lying areas of Niigata City. The soils in and around this city consist of recently reclaimed land and young sedimentary deposits having low density and a shallow ground water table. About 2,000 houses in Niigata City were totally destroyed; more than 200 reinforced concrete buildings tilted rigidly without appreciable damage to the structure (Fig. 2.4).

In most cases the liquefied sediments are sand or silty sand. However, well-graded gravel has increasingly been witnessed to liquefy during recent earthquakes. During the 1983 Borah Peak earthquake in Idaho, for example, fluvial sandy gravel liquefied extensively (Youd et al., 1985). Another example is the extensive liquefaction of reclaimed land in Kobe during the 1995 Hyogoken Nambu earthquake in Japan (Kokusho, 2007), which was filled with gravel-sized granules and fines of decomposed granite.

2.3 Laboratory Studies

Terzaghi's principle of effective stress (see Appendix 3), first proposed in the early twentieth century (Terzaghi, 1925), laid the foundation for soil mechanics and later for earthquake engineering. The structural integrity of sediments, which allows the sediments to carry weight, is normally maintained through grain-to-grain contacts. Seismic shaking can disturb the grain-to-grain contacts to cause sediments to consolidate. Some weight initially carried by the sediments is then shifted to

the interstitial pore water. Since the duration of seismic shaking, normally tens of seconds, is short compared to the time required to dissipate pore pressure in the sediment, consolidation of saturated sediments occurs in an 'undrained' condition, and pore pressure builds up. As a result, the 'effective stress' supported by the sediments decreases correspondingly. If pore pressure continues to increase and the effective stress vanishes, all the weight-carrying capacity of the sediments is lost and the weight of the sediments is born entirely by the pore water and the sediments become fluid-like.

Based on the principle of effective stress, earthquake engineers have carried out a great many laboratory experiments in the past half a century to better understand the processes of undrained consolidation of saturated sediments under cyclic loading, the ensuing pore-pressure buildup, and the eventual occurrence of liquefaction. Figure 2.5 shows the changes in shear stress and pore pressure in a sand specimen under cyclic shearing at constant strain amplitude of $\pm 2 \times 10^{-3}$. Pore pressure

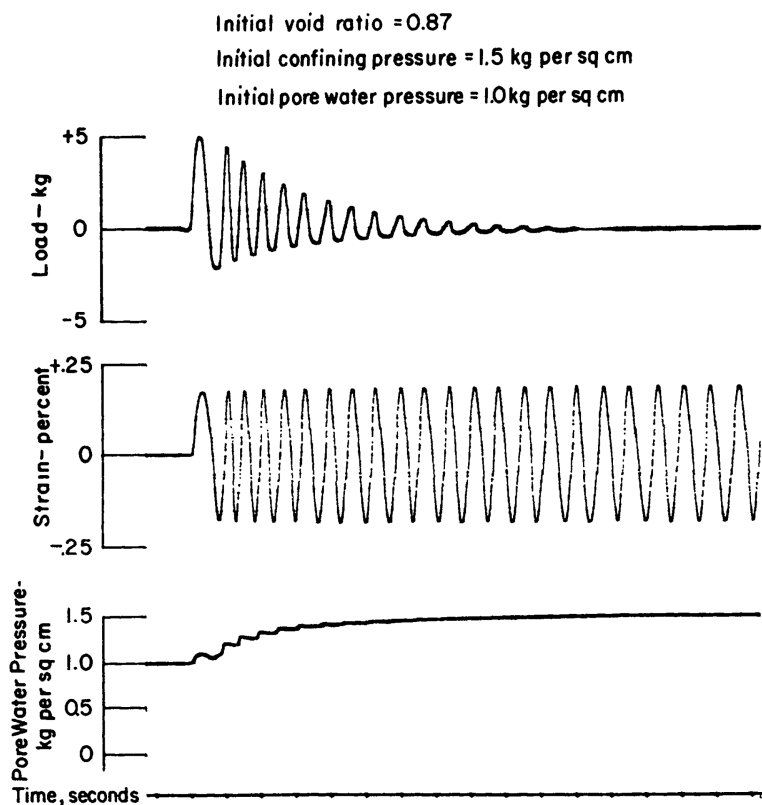


Fig. 2.5 Pore-pressure generation and axial stress in a saturated sand specimen subjected to cyclic shearing at constant strain of $\pm 2 \times 10^{-3}$. The sediment specimen had an initial dry density of 87%. The sample was subjected to a confining pressure of 15 KPa and an initial pore pressure of 10 KPa. Note that the axial stress declined with increasing number of cycles, showing a continued weakening. The rate of pore pressure increase also declined with increasing number of cycles (From Seed and Lee, 1966)

increased gradually from the beginning of shearing until it reaches the magnitude of the confining pressure. With the increasing pore pressure, the sample weakens as demonstrated by the diminishing shear stress it supports. The sample fluidizes when its shear strength approaches zero and the pore pressure approaches the magnitude of the confining pressure. These changes are complimentary to those obtained in the constant stress experiment (Figs. D.4 and D.5).

In the following Sect. 2.3.1 we review the important developments in cyclic loading experiments designed to understand the processes of liquefaction under seismic shaking. In the next subsection we summarize the experimental results on the dissipated energy required to initiate liquefaction by undrained consolidation. This provides the basis for the discussion in Sect. 2.4 in which we show that undrained

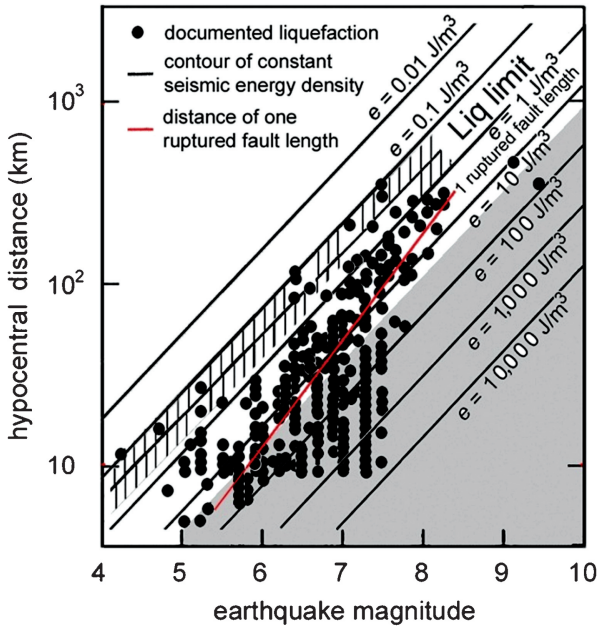


Fig. 2.6 Global dataset for hypocentral distance of documented liquefactions, shown in *solid circles*, is plotted against earthquake magnitude; hatched band marks the threshold distance of liquefaction (i.e., the liquefaction limit) as a function of earthquake magnitude (Wang et al., 2006). *Black lines* are contours of constant seismic energy densities (Eq. 2.4). *Grey line* is the empirical relation between the epicentral distance of 1 ruptured fault length and earthquake magnitude (see text for explanation), which defines the outer boundary of the ‘near field’. The upper boundary of the *shaded area* corresponds to a contour with $e = e_u = 30 \text{ J/m}^3$ – the minimum dissipated energy density required to initiate consolidation-induced liquefaction in sensitive sediments (see text for explanation); thus the *shaded area* is associated with seismic energy densities greater than 30 J/m^3 . Note that the shaded region lies mostly in the near field; note also that abundant liquefactions occurred at distances beyond the near field up to distances of several ruptured fault lengths, i.e., the ‘intermediate field’, with the liquefaction limit located where the seismic energy density falls in a range between 0.1 and 1 J/m^3 (From Wang, 2007)

consolidation may occur only in the near field of an earthquake and that, beyond the near field, the seismic energy density may be too small to induce undrained consolidation. On the other hand, a great number of liquefaction features have been documented beyond the near field (Fig. 2.6; Wang, 2007). Thus, while Terzaghi's principle may explain the occurrence of liquefaction within the near field, a new mechanism is required to explain the occurrence of liquefaction beyond the near field.

2.3.1 Cyclic Loading Experiments

Much of the current understanding of the mechanism of liquefaction is based on the results of a large number of laboratory experiments in geotechnical engineering, in which saturated sediments are subjected to cyclic loading (e.g., National Research Council, 1985). The major objective of these studies is to quantify how pore pressure changes in the cyclically loaded sediments and how sediments eventually liquefy. Despite the different experimental designs, i.e., cyclic torsional shearing of cylinders in a triaxial loading apparatus (e.g., Liang et al., 1995) and special shake tables designed to operate in large centrifuge machines (e.g., Dief, 2000), the sediment samples are all hydraulically isolated from their surroundings, i.e., the experiments are conducted in an undrained condition. The results of these experiments have been variously applied to evaluate the liquefaction potential of sediment sites, either using a threshold stress as an indicator (e.g., Seed and Idriss, 1967; Youd, 1972), or a threshold strain (Dobry et al., 1982; Vucetic, 1994; Hsu and Vucetic, 2004), or the dissipated energy as a criterion (Nemat-Nasser and Shokooh, 1979; Berrill and Davis, 1985; Law et al., 1990; Figueroa et al., 1994; Liang et al., 1995; Dief, 2000; Green and Mitchell, 2004). The last of these, i.e., the dissipated energy, can be directly compared with the seismic energy in the field and is most directly relevant to the present discussion.

Nemat-Nasser and Shokooh (1979) introduced the concept of dissipated energy for the analysis of densification and liquefaction of sediments. Berrill and Davis (1985), Law et al. (1990) and Figueroa et al. (1994) established relations between pore pressure development and the dissipated energy during cyclic loading to explore the use of energy density in the evaluation of the liquefaction potential of sediments. Liang et al. (1995) conducted torsional triaxial experiments on hollowed cylinders of sand to examine the effect of relative density, initial confining pressure and shear-strain magnitude and determined the energy per unit volume (i.e., dissipated energy density) accumulated up to liquefaction; they showed that the dissipated energy density required to induce liquefaction is a function of the relative density of the sediment and the confining pressure. Dief (2000) carried out shake table experiments in a centrifuge with scaled models under a wide range of physical conditions. Dief (2000) also determined the energy density accumulated up to the point of liquefaction and compared the results with those of earlier studies.

2.3.2 Dissipated Energy for Liquefaction by Undrained Consolidation

Given the experimental time-histories of shear stress and strain (e.g., Fig. D.5), the cumulative dissipated energy density required to initiate liquefaction by undrained consolidation may be determined by performing the following integral (Berrill and Davis, 1985):

$$e_u = \int_0^t \tau d\gamma \quad (2.1)$$

where τ is the shear stress, γ the shear strain, and the integration extends from the beginning of the cyclic loading to the onset of liquefaction. For the most part, the stress-strain relation varies with each loading cycle, thus the integral can only be evaluated by numerical integration of the experimental stress and strain time histories.

Through such integration, Liang et al. (1995) estimated a dissipated energy density for liquefaction ranging from 290 to 2,700 J/m³ for sediments with relative densities ranging from 51 to 71% subjected to confining pressures ranging from 41 to 124 KPa; Dief (2000) estimated a dissipated energy density ranging from 470 to 1,700 J/m³ for relative densities ranging from 50 to 75% subjected to an equivalent confining pressures of ~ 30 KPa; and Green and Mitchell (2004) obtained a dissipated energy density ranging from 30 to 192 J/m³ for *clean sand* at an effective confining pressure of 100 KPa. Thus there is a wide range in the dissipated energy density required to induce liquefaction for the ranges of sediment type, relative density and confining pressure studied. The large discrepancies among the different studies may be expected in view that sediments vary widely in their hydro-mechanical properties and the wide range of experimental conditions. Assuming that the sediment types, the relative density, and confining pressures in these studies are representative for the field conditions relevant to liquefaction, we may take the low value 30 J/m³, as determined by Green and Mitchell (2004) for clean sand, as the lower bound for the dissipated energy density required to induce liquefaction in the field. The lower bound imposes a threshold seismic energy density required to initiate *consolidation-induced* liquefaction in the field, which, in turn, sets a maximum distance from the earthquake source, as shown in the next section, beyond which consolidation-induced liquefaction may not be expected. The maximum distance so estimated may then be compared with the actual occurrence of liquefaction in the field to verify the hypothesis of undrained consolidation.

2.4 Liquefaction Beyond the Near Field

In Fig. 2.6 we show a recent compilation of global data for liquefaction (Wang, 2007), in which the hypocentral distance r of the documented liquefaction site is plotted against earthquake magnitude M . These parameters, i.e., r and M , are used

to characterize the liquefaction occurrences because the majority of documentations (many historical) do not note the style of faulting, the directivity of fault rupture, or the distance to the ruptured fault, nor do they make a distinction among the different magnitude scales. As shown by several authors (Kuribayashi and Tatsuoka, 1975; Ambraseys, 1988; Papadopoulos and Lefkopulos, 1993; Galli, 2000; Wang et al., 2006; Wang, 2007), the occurrence of liquefaction at a given M is delimited by a maximum distance – the liquefaction limit. Since the susceptibility of sediments to liquefaction varies significantly with sediment type and grain size (Seed and Lee, 1966; National Research Council, 1985; Dobry et al., 1982; Hsu and Vucetic, 2004), sediments that liquefy at the liquefaction limit are likely those with the least resistance.

Also shown in Fig. 2.6 is an empirical relation between M and the epicentral distance equal to 1 ruptured fault length for all subsurface fault types (Wells and Coppersmith, 1994). While a large number of the documented liquefactions occur in the near field, i.e., at epicentral distances less than or equal to one ruptured fault length, an equally large number occurred beyond the near field at distances up to several ruptured fault lengths.

2.4.1 Seismic Energy Density as a Metric for Liquefaction Distribution

The seismic energy density e at a site during ground shaking may be estimated from the time histories of particle velocity v of the ground motion as recorded by strong-motion seismometers (Lay and Wallace, 1995):

$$e = \frac{1}{2} \sum_i \frac{\rho}{T_i} \int v_i(t)^2 dt, \quad (2.2)$$

where the summation is taken over all the relevant modes of the ground vibrations, ρ is density, and T_i and v_i are, respectively, the period and the velocity of the i^{th} mode. Since most energy in the ground motion resides in the peak ground velocity, PGV , we may simplify the above relation to

$$e \sim PGV^2. \quad (2.3)$$

This relation was shown to be consistent with field data in Wang et al. (2006).

Using $\sim 30,000$ strong-motion records for southern California earthquakes, Cua (2004) showed that the peak ground velocity attenuates with the epicentral distance as $\sim 1/r^{1.5}$ for sediment sites. It follows from (2.3) that,

$$e(r) \cong A/r^3, \quad (2.4)$$

where A is an empirical parameter for southern California. Note that this relation can only be taken as a first-order approximation (i.e., a point-source approximation

for the earthquake) because the effect of source dimension and rupture directivity, which become important in determining the distribution of seismic energy in the near field, are not included. Given this approximation, the total seismic energy of an earthquake, E , is related to the energy density at $r = 1$ m, thus to A , by

$$E = \frac{4\pi}{3} e (r = 1 \text{ m}) \cong \frac{4\pi}{3} A \quad (2.5)$$

Hence $A \cong 3E/4\pi$; inserting this into (2.4) we have:

$$e(r) \cong \frac{3E}{4\pi} r^{-3}. \quad (2.6)$$

Note that this relation is entirely empirical and includes both the geometrical and physical dissipation of the seismic energy. Because of its empirical nature, this relation is strictly valid only for southern California, and may show significant differences from region to region. But, for the reason that no similar relation is yet available elsewhere, we will take it as generally valid.

Combining the above relation with Bath's (1966) empirical relation between E and earthquake magnitude M , we obtain the following empirical relation among e , r and M (Wang, 2007):

$$\log r = 0.48 M - 0.33 \log e(r) - 1.4 \quad (2.7)$$

where r is in km. This relation is plotted in Fig. 2.6 as straight lines for different values of e .

Studies show that the threshold strain required to initiate undrained consolidation in the field is the same as that in the laboratory (Hazirbaba and Rathje, 2004). Thus it may be justified to compare the seismic energy density in the field with the laboratory-based dissipated energy required to initiate liquefaction. Given the discussion in the last section on the laboratory-determined dissipated energy required to initiate liquefaction, we may tie the *maximum* distance of liquefaction occurrence due to undrained consolidation with the contour of $e = e_u = 30 \text{ J/m}^3$, shown by the upper boundary of the shaded area in Fig. 2.6. As the figure shows, this *maximum* distance corresponds closely with the hypocenter distance of ~ 1 ruptured fault length, i.e., the outer boundary of the near field. Thus undrained consolidation may account for liquefaction only in the near field. However, as noted earlier, abundant liquefaction are documented at distances far beyond the near field (Fig. 2.6), where the seismic energy density is much below the threshold energy required to induce undrained consolidation. At the maximum distance of liquefaction occurrence, i.e., the liquefaction limit, the seismic energy density declines to $\sim 0.1 \text{ J/m}^3$ which is two orders of magnitude smaller than the threshold energy required to induce undrained consolidation.

2.4.2 Mechanism for Liquefaction Beyond the Near Field

Since the seismic energy density beyond the near field is smaller than the threshold energy density required to initiate consolidation, a different mechanism is needed to account for the occurrence of liquefaction in the intermediate field. An important point to note is that, even though the seismic energy density in the intermediate field is not large enough to induce sediment liquefaction by undrained consolidation, it nonetheless may move the sediments towards a critical state so that they may liquefy if an additional increment of pore pressure becomes available to push the sediments over the liquefaction limit. In the following, we examine whether the spreading of pore pressure from a source to surrounding sediments may be a viable mechanism to provide this additional pore pressure needed to produce liquefaction.

As discussed in Chap. 5, changes of the water level in wells have long been reported after earthquakes and taken to indicate a change in the pore pressure in the groundwater system. Persuasive evidence has become available recently to show that earthquakes can enhance permeability to allow a spread of pore pressure from one part of the hydraulic system to another. Figure 2.7, for example, shows the water-level records from closely spaced wells which monitored the water levels in vertically separated aquifers in central Taiwan before and after the 1999 Chi-Chi earthquake (Water Resource Bureau, 1999). Before the earthquake, the water levels in these wells were distinct, showing that the different aquifers were hydraulically

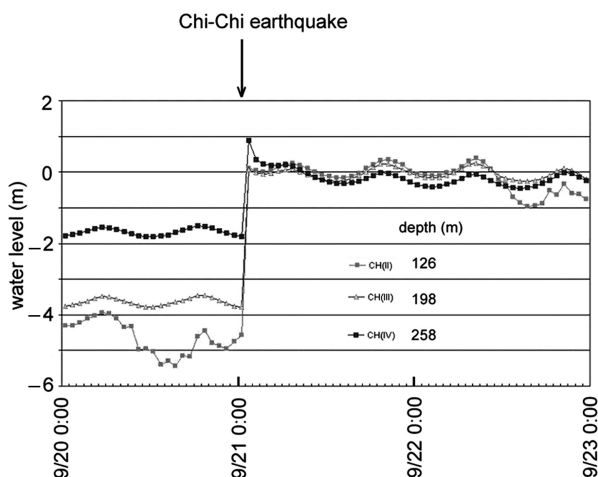


Fig. 2.7 Water-levels in three confined aquifers at a hydrological station (Chuanhsin) in central Taiwan before and after the Chi-Chi earthquake (Water Conservancy Agency, 1999). Hourly data are displayed; different symbols show data for different aquifers. Fine ticks on the horizontal axis are hourly markings; the depths of the aquifers are also given. The sinusoidal oscillations in water levels correspond to the semidiurnal tides. The water levels in the three aquifers were distinct before the earthquake, but became nearly identical after the earthquake, suggesting the aquifers were hydraulically connected by enhanced vertical permeability during the earthquake (From Wang, 2007)

isolated from each other; following the earthquake, however, the water-levels in all these wells came to the same level, suggesting that there was an enhanced *vertical* permeability that connected the different aquifers during the earthquake. The above observation was made in the near field of the earthquake. In the intermediate field, Elkhoury et al. (2006) used the tidal response of water level in wells to measure permeability over a 20-year period and showed distinct transient shifts in the phase of the water level in response to earthquakes at distances beyond the near field. They interpreted these phase shifts in terms of an enhanced permeability induced by earthquakes and attributed the increase in permeability to the removal of colloidal particles from clogged fractures by the seismic waves (Brodsky et al., 2003).

As argued above, the occurrence of consolidation-induced liquefaction may be limited to the near field of an earthquake. To explain the occurrence of liquefaction beyond the near field, we invoke the mechanism of pore-pressure spreading from nearby sources to sediment sites. Since pore-pressure heterogeneity may be the norm in the field, an enhancement of permeability among sites of different pore pressures may cause pore pressure to spread (Roeloffs, 1998; Brodsky et al., 2003; Wang, 2007). Such processes may provide an additional increment of pore pressure to push some critically stressed sediments over the critical state to become liquefied. A corollary to this hypothesis is that during the evaluation of the liquefaction potential of a site, it may be important to consider the hydrogeologic environment of the site, in addition to evaluating the liquefaction susceptibility of the site in isolation.

Finally, we note that the seismic energy density for liquefaction at the threshold distance is minute ($\sim 0.1 \text{ J/m}^3$). What is the mechanism(s) that may cause permeability to increase at such small seismic energies? The model proposed by Brodsky et al. (2003), that the removal of colloidal particles from clogged fractures may enhance the permeability of fractured rocks, implies that a minute amount of seismic energy may suffice to initiate a redistribution of pore pressure. Direct laboratory measurements, however, are needed to quantify the process in order to test this hypothesis. More detailed discussion on the mechanism of removal of colloidal particles from clogged fractures and pores is given in Chap. 5 (Sect. 5.3.3).

2.5 Experiment at Wildlife Reserve, California

The Wildlife liquefaction array was a field experimental array established in 1982 on a flood plain in southern California, about 10 km southeast of the Salton Sea (Fig. 2.8a), and designed specifically to study liquefaction processes. The array (Fig. 2.8b) consisted of two 3-component accelerometers placed at the surface and in a cased borehole at a depth of $\sim 7 \text{ m}$, and six pore-pressure transducers placed around the accelerometers at various depths up to 12 m. Both the M6.2 Elmore earthquake and the M6.6 Superstition Hills earthquake triggered the accelerometers, but only the latter earthquake triggered liquefaction at the array, which caused sand boils with eruptions of water and sediments. Extensive ground cracking implied lateral spreading at the array (Holzer et al., 1989).

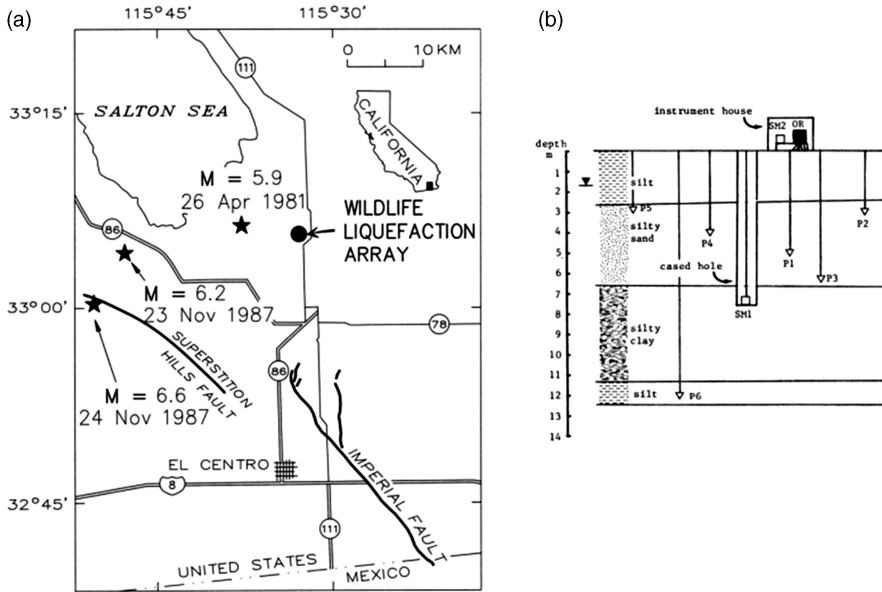
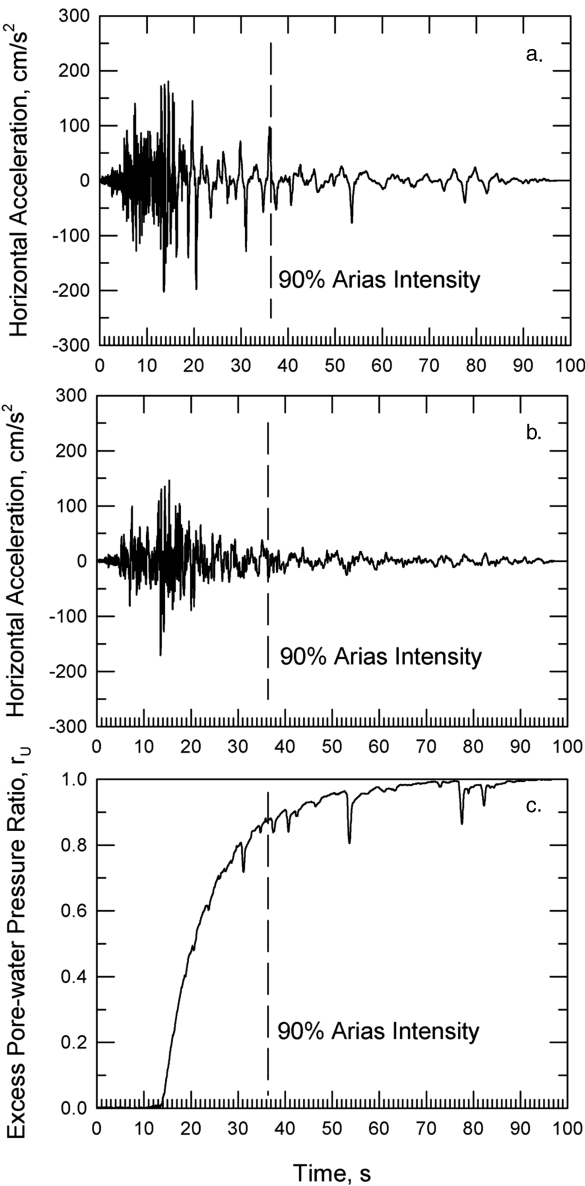


Fig. 2.8 (a) Location map of the Wildlife Reserve Array and earthquake epicenters. M6.6 is the 1987 Superstition Hills earthquake, M6.2 is the 1987 Elmore Ranch earthquake, and M5.9 is the 1981 Westmorland earthquake. (b) Stratigraphic cross-section of array and schematic of instrument deployment. In plain view, pore-pressure transducers (denoted by P) are equally spaced on the perimeter of a circle with a diameter of 9.1 m. Accelerometers are near center of circle (From Holzer et al., 1989)

The in situ time histories of pore pressure and acceleration at Wildlife Reserve Array during and following the Superstition Hills earthquake reveal a complex interaction among ground shaking, pore pressure buildup and liquefaction (Fig. 2.9). For the convenience of description, Zeghal and Elgamal (1994) divided the recorded time histories of ground shaking during the Superstition Hills earthquake into four stages: Stage 1 (0.0–13.7 s): Ground acceleration was below ~ 0.1 g and pore water pressure buildup was small. Stage 2 (13.7–20.6 s): Strongest shaking occurred, with peak accelerations of 0.21 and 0.17 g at the surface and downhole instruments, respectively. Pore-water pressure increased rapidly, with small instantaneous drops. Stage 3 (20.6–40.0 s): Accelerations declined and stayed below 0.06 g. Pore-water pressure continued to increase at a high rate. Stage 4 (40.0–96.0 s): Ground acceleration was very low (~ 0.01 g), but excess pore pressure continued to rise, though at a slower rate, reaching the maximum pore pressure at 96 s. Thus a large portion of excess pore pressure at the Wildlife Reserve Array developed after the stronger, high-frequency ground motion had abated, and liquefaction did not occur until the earthquake was almost over (Holzer et al., 1989).

Many other investigations of the Wildlife recordings have been conducted (e.g., Zeghal and Elgamal, 1994; Youd and Carter, 2005; Holzer and Youd, 2007). Zeghal

Fig. 2.9 Time histories of (a) north-south surface accelerations, (b) north-south downhole accelerations, and (c) excess pore pressure ratio recorded by piezometer P5 during and following the Superstition Hills earthquake. The downward spikes show rapid and transit decreases in pore-pressure. Ratio was calculated by dividing recorded values by the value at 97 s (From Holzer and Youd, 2007)



and Elgamal (1994) first demonstrated that the buildup of pore pressure was accompanied by a progressive softening of the sediments. Double-integrating the surface and downhole acceleration records leads to the time histories of displacements at the surface and at the downhole depth. The acceleration and displacement records may then be used to calculate the time histories of shear stress and the average shear strain (Zeghal and Elgamal, 1994). An example, recalculated by Holzer and Youd

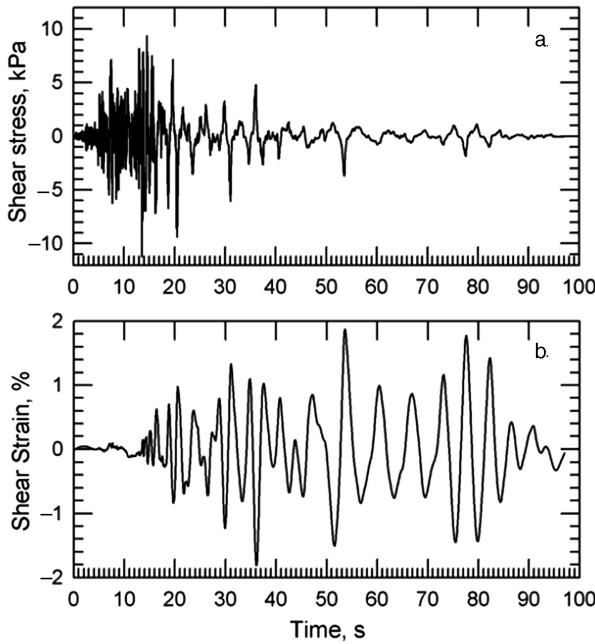


Fig. 2.10 Time histories of (a) north-south shear stress and (b) north-south shear strain at the Wildlife Reserve array during the Superstition Hills earthquake (From Holzer and Youd, 2007)

(2007), is shown in Fig. 2.10. An interesting result is that large amplitude (up to $\sim 2\%$) long period (~ 5.5 s) cyclic shear strains continued to affect the sediments long after the high-frequency acceleration had abated. It shows that the sediments had softened so much that they underwent large shear deformations at very small shear stresses.

The progressive softening of sediments is best demonstrated by plotting the time history of shear stress against that of shear strain (Fig. 2.11), recalling that the slope of the stress-strain curve may be identified as the ‘rigidity’ of the sediments. At the onset of rapid pore-pressure increase, i.e., at 13.6 s (Fig. 2.9), the stress-strain curve shows steep slopes, i.e., high rigidity. With progressive increase in time, the slopes of the stress-strain curves rapidly decreased, showing that the sediments softened. Near the strain extremities, however, the slopes increase suddenly, showing that the sediments stiffened once more. This latter stiffening was attributed to strain-hardening (Zeghal and Engam, 1994) and may be related to the rapid and transient decreases in pore pressure as recorded by the piezometers (Fig. 2.9; some of the decreases are labeled in Fig. 2.11), which, in turn, may be interpreted as a consequence of dilatancy in the strain-hardened sediments. With progressive softening, the activation of strain-hardening requires progressively greater amount of shear strain. As a result, large deformation may be induced by very small disturbances and the sediments fluidize.

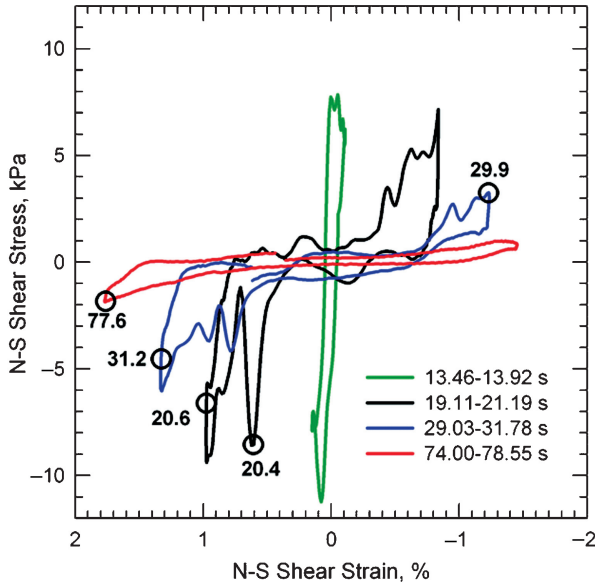


Fig. 2.11 Four hysteresis curves between shear stress and shear strain at different time segments. The times of instantaneous drop of pore pressure as recorded by piezometer P5 are labeled on the hysteresis curves (From Holzer and Youd, 2007)

It has been a challenge to explain why pore pressure continued to increase long after the ground acceleration had abated (e.g., Holzer et al., 1989; Holzer and Youd, 2007). One explanation is offered by the discussion in the last section. We note that the distance between the Wildlife Reserve Array and the epicenter of the M6.6 Superstition Hills earthquake (31 km, Holzer et al., 1989) is beyond the near field of the earthquake (<20 km); thus the seismic energy density at the Wildlife Reserve Array at the time of the earthquake may be too small to induce undrained consolidation, even in the most sensitive sediments. Second we note that the rise in pore pressure (Fig. 2.9c) was gradual and sustained, distinct from that caused by undrained consolidation which would have appeared as a steplike increase coincident with the strongest ground shaking (Roeloffs, 1998; Wang and Chia, 2008). The gradual and sustained change of pore pressure, however, can be readily explained by the diffusion of pore pressure from a nearby source that connected to the Wildlife Reserve Array through an earthquake-enhanced permeability, as discussed in the previous section. Under such condition, the duration of the pore-pressure increase does not depend upon the duration of ground shaking, but is rather a function of the distance between the pore-pressure source and the Wildlife Reserve Array as well as the permeability of the earth media between the two locations, thus explaining the continued pore-pressure buildup long after the ground acceleration had diminished. A different explanation offered by Holzer and Youd (2007) is that the strong ground shaking had initiated consolidation and thus pore-pressure increase in the sediments, and consolidation may have continued afterwards under the action of the

long-period surface waves that arrived after the ground shaking had abated. If so, the sediments at the Wildlife Reserve Array would have to be more sensitive than the most sensitive sediments so far tested in the laboratory. An interesting point of this model is the positive feedback between pore-pressure buildup and sediment weakening, i.e., sediments which have been progressively weakened by rising pore pressure during seismic loading may continue to consolidate and generate pore pressure at progressively lower stresses, which further weakens the sediments.

In summary, the Wildlife Reserve Array experiment demonstrated that the occurrence of liquefaction is the culmination of a complex sequence of interactions among ground shaking, sediment deformation and pore-pressure redistribution and/or buildup. An increase in pore pressure weakens the sediment framework; this leads to greater deformation of the sediments. Continued increase in pore pressure may occur due to enhanced permeability connecting the sediments to a nearby source, or possibly by continued consolidation. This process continues at low frequency and very small shear stresses until the sediments liquefy.

2.6 Dependence of Liquefaction on Seismic Frequency

The period of seismic waves recorded near some liquefaction sites ranges from less than a second to many tens of seconds. Thus it is important to investigate whether the initiation of liquefaction depends on the frequency of seismic waves and, if so, how does it depend on the seismic frequency.

Established engineering methods frequently use the peak ground acceleration (PGA) as an index to predict liquefaction risk (Seed and Idriss, 1971). This is because PGA is proportional to the maximum shear stress induced in the sediment (Terzaghi et al., 1996). On the other hand, Midorikawa and Wakamatsu (1988) calculated PGA and PGV at ~130 liquefaction sites and found that the occurrence of liquefaction is better correlated with the calculated PGV than with PGA. This result implies that liquefaction may be more sensitive to the low frequency components of the ground motion. This is because the integration of the acceleration records to calculate velocity filters out higher frequencies, so PGV is more dominated by low frequencies than PGA. In the following we test these models by using the occurrence of liquefaction, groundwater-level changes, and strong-motion records from central Taiwan during the Chi-Chi earthquake (Wang et al., 2003; Wong and Wang, 2007).

2.6.1 Field Observation from Taiwan

The 1999 M_w 7.6 Chi-Chi earthquake (Fig. 2.12) caused widespread liquefaction on the Choshui Alluvial Fan and the surrounding area (Fig. 2.13). An extensive network of strong-motion seismographs and a similarly extensive network of hydrologic monitoring wells were installed on the fan (Fig. 2.12) which captured both the ground motion and the concurrent groundwater level changes during and after the

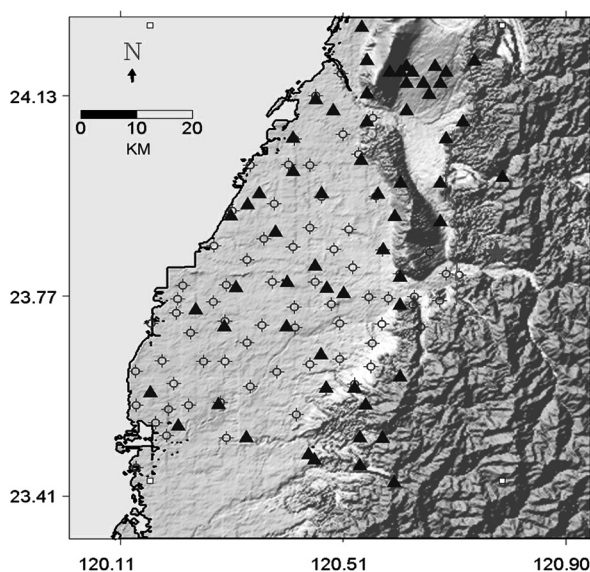


Fig. 2.12 Distribution of strong-motion stations (*solid triangles*) and hydrologic stations (*open circles*) on the Choshui alluvial fan (i.e., the flat fan-shaped area to the west of the hilly area) and nearby areas in western Taiwan. At each of the stations, there are one to five monitoring wells drilled to different depths up to 300 m. *Red star* marks the epicenter of the Chi-Chi earthquake, and *red curve* shows the ruptured fault in the earthquake (From Wang et al., 2006)

earthquake. These data provide a rare opportunity to investigate the field relationship among liquefaction, ground motion and groundwater level changes.

Taiwan is a north-south elongated island arc formed by the oblique collision between the Luzon volcanic arc on the Philippine Sea plate and the continental margin of China beginning in the late Cenozoic (Teng, 1990). The Choshui River Alluvial Fan (Fig. 2.12) is part of the Coastal Plain that lies along the western coast of the island and is covered by unconsolidated sediments of Neogene and Quaternary age, floored by a faulted basement. The Western Foothills that lie immediately to the east of the Coastal Plain, on the other hand, is a fold-and-thrust belt of consolidated sedimentary rocks, with virtually no loose sediments (Ho, 1988). The 1999 Chi-Chi ($M_w = 7.5$) earthquake, the largest to hit Taiwan in the last century, ruptured the Western Foothills along a ~ 80 km fault on the east of the Choshui River fan (Fig. 2.12).

Liquefaction was widespread in and near Yuanlin on the Choshui Alluvial Fan and further east along the ruptured fault (Fig. 2.13). The figure shows that the liquefaction sites on the Choshui River fan are closely associated with the largest coseismic rise of the groundwater level in the uppermost aquifer. No monitoring wells were installed in the basins east of the Choshui River fan; thus a similar comparison between pore pressure rise and the distribution of liquefaction cannot be made there.

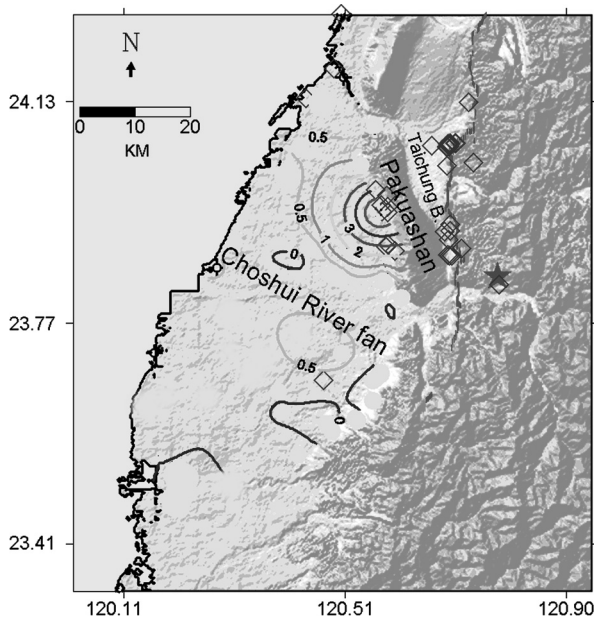


Fig. 2.13 Contours (in m) of the coseismic changes in groundwater level in the *topmost* aquifer in the Choshui alluvial fan. *Open diamond* show sites of liquefaction. Note that, on the Choshui alluvial fan, most liquefaction sites occurred in an area where the rise in groundwater level was above 2 m (Modified from Wang et al., 2006)

In order to test the frequency-dependence of pore-pressure development and liquefaction Wang et al. (2003) and Wong and Wang (2007) calculated the spectral acceleration, S_a , and spectral velocity, S_v , defined as the maximum response of a harmonic oscillator with a given damping coefficient with resonant frequency to the ground motion (Jennings, 1983). S_a and S_v were calculated at 5% damping at the location of each seismometer. Values for S_a and S_v throughout the region were then interpolated from the S_a and S_v values at the seismic stations (Fig. 2.13) using a kriging procedure. As an example, Fig. 2.14 shows maps of the spatial distribution of S_a at different frequencies together with the spatial distribution of the liquefaction sites. Visual inspection of the maps shows that there is a strong correlation between the liquefaction sites and S_a occurs at 0.5 and 1 Hz, but not at 2 Hz. A similar result occurs between the spatial distribution of S_v (not shown) and the liquefaction sites.

A more quantitative test of the above correlation of liquefaction with seismic wave frequency may be provided by plotting the t -values for the correlations of water level increase (i.e., pore pressure increase) with S_a and S_v over a range of frequencies in which liquefaction is mostly likely to occur. Calculations were made from $\sim 10^{-3}$ to $\sim 10^2$ Hz, but only a section of this range is shown in Fig. 2.15 for clarity. In general, S_a and S_v below about 0.8 Hz are more strongly correlated with the water-level increase than those above 0.8 Hz. The strength of the correlation peaks at 0.3–0.4 Hz, but declines rapidly at lower frequencies (Wong and Wang, 2007).

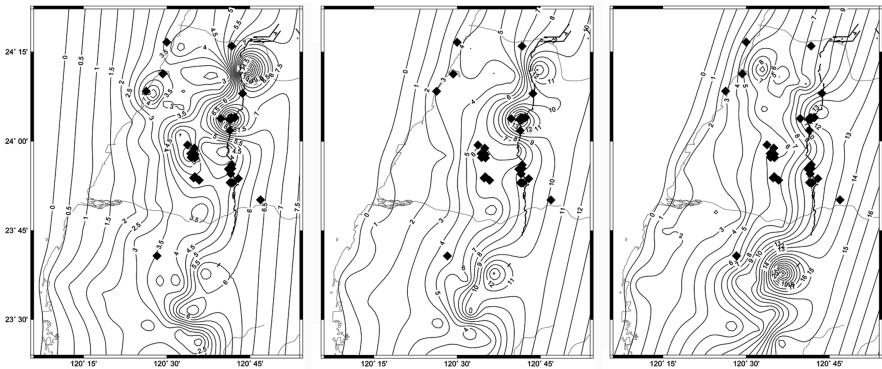


Fig. 2.14 Contours of S_a at 0.7 Hz (a), 1 Hz (b) and 2 Hz (c) during the Chi-Chi earthquake, plotted together with the distribution of liquefaction sites in solid diamonds. Note the strong correlation between liquefaction sites and S_a at 0.7 Hz and the weak correlation at 2 Hz (From Wong and Wang, 2007)

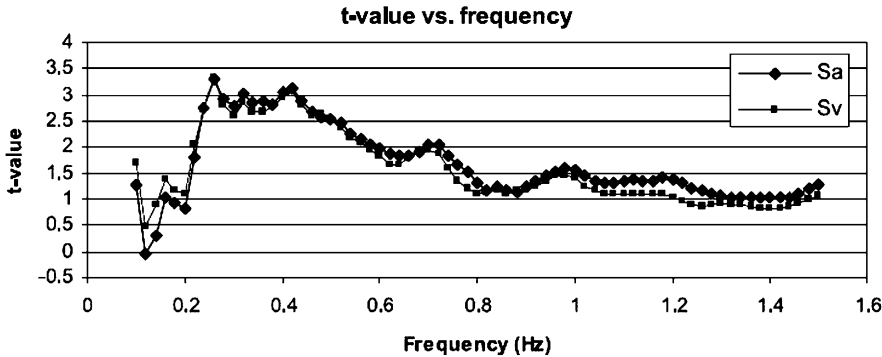


Fig. 2.15 t-values of the correlation of the water-level increase with S_a and S_v over a range of frequencies from 0.1 to 1.5 Hz, which pore pressure increases and liquefaction are typically attributed (From Wong and Wang, 2007)

2.6.2 Laboratory Studies

Only a few laboratory studies examined the dependence of liquefaction on the frequency of the seismic loads. Yoshimi and Oh-Oka (1975) conducted a series of cyclic shear tests under undrained conditions to determine the conditions to induce liquefaction in saturated sands. Most specimens in their experiments had a relative density, i.e., the ratio of the *density* of a specimen to the average *density* of the solid grains, of approximately 40%, and the frequency of the cyclic shear stress ranged from 1 to 12 Hz. They found that liquefaction failure became imminent when the ratio of the peak shear stress to the vertical effective stress reached a certain critical value, but the condition to induce liquefaction was nearly independent of the frequency of the cyclic shear stress from 1 to 12 Hz.

Sumita and Manga (2008) measured the rheology of non-Brownian particle suspensions under oscillatory shear at frequencies ranging from 0.1 to 10 Hz. A rheological transition was found to occur at a shear strain threshold of 10^{-4} , whereby the shear modulus of the viscoelastic suspension reduces sharply. This transition is in excellent correspondence with the threshold shear strain determined in geotechnical engineering experiments where excess pore pressure begins to develop and the shear modulus of the sediments begins to decline (Dobry et al., 1982; Vucetic, 1994; Hsu and Vucetic, 2004, 2006). Sumita and Manga (2008) found no dependence of the threshold shear strain on the frequency of shearing from 0.1 to 10 Hz.

Thus the field results and laboratory results on the dependence of liquefaction on frequency appear to be in conflict. On the one hand, existing laboratory results show little frequency-dependence of liquefaction; on the other hand, in situ studies of seismically instrumented liquefaction sites show an association of liquefaction with low-frequency ground motions.

2.6.3 Numerical Models

Using dynamic numerical models with nonlinear constitutive relations for sediments, Popescu (2002) and Ghosh and Madabhushi (2003) showed that the association of liquefaction and low-frequency ground motion may be due to sediment softening induced by ground motions. They also suggest a spectra-dependent feedback loop for liquefying sediments: low frequency excitation causes ground softening and pore pressure increases more efficiently than for high frequency excitation. This softening in turn reduces the resonant frequency of the sediment column, amplifying low frequency motions and damping high frequency motions, leading to further softening and pore pressure increases, possibly leading to liquefaction.

Kostadinov and Towhata (2002) proposed a linearly elastic model of one dimensional wave propagation that suggests liquefaction may occur when the sediment column reaches a resonant state. Similarly, Bachrach (2001) used a dynamic poroelastic model to simulate the effect of P-waves on pore-pressure buildup and liquefaction near the resonant frequency of sediment columns.

Further in situ, laboratory, and theoretical work are required to evaluate the dependence of pore-pressure buildup and liquefaction on the frequency of seismic waves. If the frequency dependence is due to resonance in the soil, as theoretical models suggest, local hydrologic and geologic conditions would affect ground motion frequencies.

The roles that different types of seismic waves play in inducing liquefaction also needs to be better investigated. Finally, to make predictions regarding liquefaction at particular sites, results must be integrated with site-specific geotechnical data. This requires the development of predictive theories of liquefaction that incorporate both the seismic spectral information of the ground motion, as well as geotechnical information such as SPT and CPT. Such predictions should be verified with data from earthquake-affected sites where both geotechnical data and ground motion data are available.

2.7 Concluding Remarks

Earthquake-induced liquefaction has been studied by earthquake engineers based on Terzaghi's concept that consolidation of loose sediments raises pore pressure which eventually causes liquefaction. Here we show that, while this mechanism may be valid in the near field of an earthquake, the energy of seismic waves at distances beyond the near field may be too small to induce consolidation, even in the most sensitive sediments. Hence a new mechanism may be needed to explain the abundant occurrences of liquefaction beyond the near field. Here we proposed a redistribution of pore pressure due to earthquake-enhanced permeability as a mechanism to explain these occurrences. The proposed mechanism is supported by evidence that pore pressure in the field is often heterogeneous at a local scale and that seismic waves can enhance the permeability of shallow crust at distances far beyond the near field. Thus an enhanced permeability during an earthquake may connect sites of different pore pressures in the shallow crust, which were hydraulically isolated from each other before the earthquake, allowing pore pressure to redistribute. This redistribution may raise the pore pressure at some sites to facilitate liquefaction.

An unresolved issue is the complex relationship between liquefaction and the frequency of seismic waves. Current results from the field and laboratories are in conflict. Future work is needed to resolve these conflicts.

References

- Ambraseys, N.N., 1988, Engineering seismology, *Earthquake Eng. Structural Dynamics*, 17, 1–105.
- Bachrach, R., A. Nur, and A. Agnon, 2001, Liquefaction and dynamic poroelasticity in soft sediments, *J. Geophys. Res.*, 106, 13515–13526.
- Bath, M., 1966, Earthquake energy and magnitude, *Phys. Chem. Earth*, 7, 115–165.
- Berrill, J.B., and R.O. Davis, 1985, Energy dissipation and seismic liquefaction in sands: Revised model, *Soils Found.*, 25, 106–118.
- Brodsky, E.E., E. Roeloffs, D. Woodcock, I. Gall, and M. Manga, 2003, A mechanism for sustained water pressure changes induced by distant earthquakes, *J. Geophys. Res.*, 108, doi:10.1029/2002JB002321.
- Cua, G.B., 2004, *Creating the Virtual Seismologist: Developments in Ground Motion Characterization and Seismic Early Warning*, Ph.D. Dissertation, Caltech.
- Dief, H.M., 2000, *Evaluating the Liquefaction Potential of Soils by the Energy Method in the Centrifuge*, Ph.D. Dissertation, Department of Civil Engineering, Case Western Reserve University, Cleveland, OH.
- Dobry, R., R.S. Ladd, F.Y. Yokel, R.M. Chung, and D. Powell, 1982, Prediction of pore water pressure buildup and liquefaction of sands during earthquakes by the cyclic strain method, *National Bureau of Standards Building Science Series*, 138, National Bureau of Standards and Technology, Gaithersburg, MD, pp. 150.
- Elkhoury, J.E., E.E. Brodsky, and D.C. Agnew, 2006, Seismic waves increase permeability, *Nature*, 441, 1135–1138.
- Figuerola, J.L., A.S. Saada, L. Liang, N.M. Dahisaria, 1994, Evaluation of soil liquefaction by energy principles, *J. Geotech. Eng., ASCE*, 120, 1554–1569.
- Galli, P., 2000, New empirical relationships between magnitude and distance for liquefaction, *Tectonophysics*, 324, 169–187.

- Ghosh, B. and S.P.G. Madabhushi, 2003, A numerical investigation into effects of single and multiple frequency earthquake motions, *Soil Dynamics and Earthquake Engineering*, 23, 691–704.
- Green, R.A., and J.K. Mitchell, 2004, Energy-based evaluation and remediation of liquefiable soils. In: M. Yegian, and E. Kavazanjian (eds.), *Geotechnical Engineering for Transportation Projects*, ASCE Geotechnical Special Publication, No. 126, Vol. 2, 1961–1970.
- Hazirbaba, K., and E.M. Rathje, 2004, A comparison between in situ and laboratory measurements of pore water pressure generation. In: *13th World Conference on Earthquake Engineering*, paper no. 1220, Vancouver.
- Ho, C.S., 1988, *An Introduction to the Geology of Taiwan*, 2nd ed., 192 pp, Taiwan: Central Geological Survey.
- Holzer, T.L., J.C. Tinsley, and T.C. Hank, 1989, Dynamics of liquefaction during the 1987 Superstition Hills, California, earthquake, *Science*, 244, 56–59.
- Holzer, T.L. and T.L. Youd, 2007, Liquefaction, ground oscillation, and soil deformation at the Wildlife Array, California, *Bull. Seis. Soc. Am.*, 97, 961–976.
- Hsu, C.C., and M. Vucetic, 2004, Volumetric threshold shear strain for cyclic settlement, *J. Geotech. Geoenviron. Eng.*, 130, 58–70.
- Hsu, C.C., and M. Vucetic, 2006, Threshold shear strain for cyclic pore-water pressure in cohesive soils, *J. Geotech. Geoenviron. Eng.*, 132, 1325–1335.
- Jennings, P.C., 1983, Engineering seismology. In: H. Kanamori, and E. Boschi (ed.), *Earthquakes: Observation, Theory and Interpretation*, Amsterdam: North-Holland.
- Kokusho, T., 2007, Liquefaction strengths of poorly-graded and well-graded granular soils investigated by lab tests. In: K.D. Ptilakis (ed.), *Earthquake Geotechnical Engineering*, Dordrecht: Springer.
- Kostadinov, M.V., and I. Towhata, 2002, Assessment of liquefaction-inducing peak ground velocity and frequency of horizontal ground shaking at onset of phenomenon, *Soil Dyn. Earthq. Eng.*, 22, 309–322.
- Kuribayashi, E., and F. Tatsuoka, 1975, Brief review of liquefaction during earthquakes in Japan, *Soils Found.*, 15, 81–92.
- Law, K.T., Y.L. Cao, and G.N. He, 1990, An energy approach for assessing seismic liquefaction potential, *Can. Geotech. J.*, 27, 320–329.
- Lay, T., and T.C. Wallace, 1995, *Modern Global Seismology*, pp. 521, San Diego: Academic Press.
- Liang, L., J.L. Figueroa, and A.S. Saada, 1995, Liquefaction under random loading: Unit energy approach, *J. Geotech. Eng.*, 121, 776–781.
- Marinatos, S.N., 1960, Helice: A submerged town of classical Greece, *Archaeology*, 13, 186–193.
- Midorikawa, S., and K. Wakamatsu, 1988, Intensity of earthquake ground motion at liquefied sites, *Soils Found.*, 28, 73–84.
- National Research Council, 1985, *Liquefaction of Soils during Earthquakes*, pp. 240, National Academy Press, Washington, DC.
- Nemat-Nasser, S., and A. Shokoh, 1979, A unified approach for densification and liquefaction of cohesionless sands in cyclic loading, *Can. Geotech. J.*, 16, 659–678.
- Obermeier, S.F., 1989, The new madrid earthquakes: An engineering-geologic interpretation of relic liquefaction features, *U.S. Geol. Surv. Prof. Pap.*, 1336-B, 114.
- Papadopoulos, G.A., and G. Lefkopulos, 1993, Magnitude-distance relations for liquefaction in soil from earthquakes, *Bull. Seism. Soc. Am.*, 83, 925–938.
- Ptilakis, K.D. (ed.), 2007, *Earthquake Geotechnical Engineering*, Dordrecht: Springer.
- Popescu, R., 2002, Finite element assessment of the effects of seismic loading rate on soil liquefaction, *Canadian Geotech. J.*, 29, 331–334.
- Roeloffs, E.A., 1998, Persistent water level changes in a well near Parkfield, California, due to local and distant earthquakes, *J. Geophys. Res.*, 103, 869–889.
- Schmidt, F.J., 1875, *Studien über Erdbeben*, pp. 360, Leipzig: Carl Scholtze.
- Seed, H.B., 1968, Landslides during earthquakes due to soil liquefaction, *J. Soil Mech. Found. Div.*, 94, 1055–1122.

- Seed, H.B., and K.L. Lee, 1966, Liquefaction of saturated sands during cyclic loading, *J. Soil Mech. Found. Div.*, 92, 105–134.
- Seed, H.B., and I.M. Idriss, 1967, Analysis of soil liquefaction: Niigata earthquake, *J. Soil Mech. Found. Div.*, 93, 83–108.
- Seed, H.B., and I.M. Idriss, 1971, Simplified procedure for evaluating soil liquefaction potential, *J. Soil Mech. Found. Div.*, 97, 1249–1273.
- Su, T.-C., K.-W. Chiang, S.-J. Lin, F.-G. Wang, and S.-W. Duann, 2000, Field reconnaissance and preliminary assessment of liquefaction in Yuan-Lin area, *Sino-Geotechnics*, 77, 29–38.
- Sumita, I., and M. Manga, 2008, Suspension rheology under oscillatory shear and its geophysical implications, *Earth Planet. Sc. Lett.*, 269, 467–476.
- Teng, L.S., 1990, Geotectonic evolution of late Cenozoic arc-continent collision in Taiwan, *Tectonophysics*, 183, 57–76.
- Terzaghi, K., 1925, *Erdbaummechanik*, Vienna: Franz Deuticke.
- Terzaghi, K., R.B. Peck, and G. Mesri, 1996, *Soil Mechanics in Engineering Practice*, 3rd ed., pp. 195, New York: John Wiley and Sons.
- Tuttle, M.P., and E.S. Schweig, 1996, Recognizing and dating prehistoric liquefaction features: Lessons learned in the New Madrid seismic zone, central United States, *J. Geophys. Res.*, 101, 6171–6178.
- Vucetic, M., 1994, Cyclic threshold of shear strains in soils, *J. Geotech. Eng.*, 120, 2208–2228.
- Waller, R.M., 1966, Effects of the March 1964 Alaska earthquake on the hydrology of south-central Alaska, *U.S. Geol. Surv. Prof. Pap.*, 544-A.
- Wang, C.-Y., 2007, Liquefaction beyond the near field, *Seismo. Res. Lett.*, 78, 512–517.
- Wang, C.-Y., and Y. Chia, 2008, Mechanism of water level changes during earthquakes: Near field versus intermediate field, *Geophys. Res. Lett.*, 35, L12402, doi:10.1029/2008GL034227.
- Wang, C.-Y., D.S. Dreger, C.-H. Wang, D. Mayeri, and J.G. Berryman, 2003, Field relations among coseismic ground motion, water level change, and liquefaction for the 1999 Chi-Chi ($M_w = 7.5$) earthquake, Taiwan, *Geophys. Res. Lett.*, 30, 1890, doi:10.1029/2003GL017601.
- Wang, C.-Y., A. Wong, D.S. Dreger, and M. Manga, 2006, Liquefaction limit during earthquakes and underground explosions – implications on ground-motion attenuation, *Bull. Seis. Soc. Am.*, 96, 355–363.
- Water Resource Bureau, 1999, *Summary Report of Groundwater Monitoring Network Plan in Taiwan, Phase I, Hydrogeology of Choshui River Alluvial Fan*, Water Resource Bureau, Ministry of Economic Affairs, Taipei, Taiwan, 240 pp (in Chinese).
- Wells, D.L., and K.J. Coppersmith, 1994, New empirical relationships among magnitude, rupture length, rupture width, rupture area, and surface displacement, *Bull. Seis. Soc. Am.*, 84, 974–1002.
- Wong, A., and C.-Y. Wang, 2007, Field relations between the spectral composition of ground motion and hydrological effects during the 1999 Chi-Chi (Taiwan) earthquake. *J. Geophys. Res.*, 112, B10305, doi:10.1029/2006JB004516.
- Yoshimi, Y., and H. Oh-Oka, 1975, Influence of degree of shear stress reversal on the liquefaction potential of saturated sand, *Soils Found. (Japan)*, 15, 27–40.
- Youd, T.L., 1972, Compaction of sands by repeated shear straining, *J. Soil Mech. Found. Div., Am. Soc. Civ. Eng.*, 98, 709–725.
- Youd, T.L., E.L. Harp, D.K. Keefer, and R.C. Wilson, 1985, The Borah Peak, Idaho, earthquake of October 28, 1983 – Liquefaction, *Earthquake Spectra*, 2, 71–89.
- Youd, T.L., and B.L. Carter, 2005, Influence of soil softening and liquefaction on spectral acceleration, *J. Geotech. Geoenviron. Eng.*, 131, 811–825.
- Zeghal, M., and A.-W. Elgamal, 1994, Analysis of site liquefaction using earthquake records, *J. Geotech. Eng.*, 120, 996–1017.



<http://www.springer.com/978-3-642-00809-2>

Earthquakes and Water

Wang, C.-y.; Manga, M.

2009, X, 225 p., Hardcover

ISBN: 978-3-642-00809-2